Powder Technology 286 (2015) 31–38

Contents lists available at ScienceDirect

Powder Technology

journal homepage: www.elsevier.com/locate/powtec

Effect of thermal stability of powdered oxide on joint penetration and metallurgical feature of AISI 4130 steel TIG weldment

Kuang-Hung Tseng *, Ya-Jie Shiu

Institute of Materials Engineering, National Pingtung University of Science and Technology, Pingtung 91201, Taiwan

ARTICLE INFO

Article history:
Received 30 March 2015
Received in revised form 4 July 2015
Accepted 28 July 2015
Available online 8 August 2015

Keywords:
Alloy steel
Joint penetration
Metallurgical feature
Powdered oxide
Thermal stability
TIG welding

ABSTRACT

This study investigated the influence of thermal stability of powdered oxides on the joint penetration of tungsten inert gas (TIG) welding of high-strength low-alloy (HSLA) steels. The microstructure and microhardness of the weldments were evaluated and the results were compared. The results shows a greater improvement in the joint penetration ability (JPA) of AISI 4130 steel TIG welds produced with MoO_3 and Cr_2O_3, as compared to TIG welds produced with Al_2O_3, MgO, and CaO. TIG welding with CaO resulted in a broadening of the arc contour, which resulted in the shape of the weld becoming relatively shallow and wide compared to TIG welding without powdered oxide. The use of powdered oxide with high thermal stability may generate a heavy slag over the surface of molten metal, acting as a barrier for thermal energy transfer from the electric arc to the molten pool during powdered oxide assisted TIG welding. Moreover, the hard microstructures formed in weld metal (WM) and partial heat-affected zone (HAZ) of AISI 4130 steel weldment exhibited a considerable microhardness value (>370 H_V).

1. Introduction

Alloy steels are more responsive to mechanical and thermal treatments than plain carbon steels. There are many types of alloy steels, where each type of steel contains higher levels of Si, Mn, Ni, Cr, Mo, V, W, and B than plain carbon steel. AISI 4130 steel is a HSLA group containing Cr and Mo as hardening alloy elements [1]. The carbon content of AISI 4130 steel is nominally 0.30%, which makes the steel very good in terms of weldability. It is widely used in structural components, which require a high strength-to-weight ratio such as aircraft engine mounts [2], oil and gas valves, or pumps. TIG welding is the most popular process for joining HSLA steel, as it creates a high quality, spatter-free weld. In TIG welding process, an electric arc is established between the refractory electrode and the metal workpiece under an inert gas atmosphere. Autogenous (without using filler metal) TIG welding is used in thin metal sections, while V, U, or X type edge preparations are needed in a relatively thick section of metal. In this case, the use of filler metal is required.

Compared to autogenous plasma arc welding (PAW) process, in an autogenous TIG welding operation, the limited joint penetration restricts its ability to join thicker metal sections (≥2.5 mm) [3,4], directly reducing its productivity. An improvement in productivity has thus been desired in the TIG welding. One of the well-known methods used to pursue this is powdered flux assisted TIG (TIG-PF) welding. TIG-PF welding provides a cost-effective way of increasing the joint penetration for thicker metal sections [5]. Compared to TIG welding without powdered oxide, TIG-PF welding has 2–3 times greater joint penetration [6], thus increasing the productivity of TIG welding by reducing the number of passes required to complete a particular joint for thicker metal sections. TIG-PF welding reduces the susceptibility to changes in the depth of the weld caused by cast-to-cast variation in stainless steels [7], and achieves a consistent joint penetration. Furthermore, TIG-PF welding does not cause degeneration in the mechanical strength of the weldment.

The composition of the flux is a critical factor in enhancing joint penetration of TIG welds [8]. The fluxes have recently become commercially available for industrial applications. There is little published data on commercially available fluxes. The fluxes with a range of compositions have been developed for TIG welding of C–Mn steels, Cr–Mo alloy steels, Ni–Cr–Mo alloy steels, and Fe–Cr–Ni alloy steels [9]. The most common fluxes used in TIG welding of steels contain oxides. Previous studies [7,8,10–15] have given an understanding of which oxides have a significant influence on the joint penetration of TIG welds. It has been observed that Fe_2O_3, CuO_2, NiO, FeO, ZnO, MoO_3, Cr_2O_3, MnO_2, SiO_2, and TiO_2, the oxides most effective at increasing joint penetration of carbon steel or alloy steel TIG weld, have a relatively low thermal stability. Thermal stability of an oxide is its ability to resist thermal decomposition at high temperature conditions. The order of thermal stability for various oxides depends on Gibbs free energy of formation in constituent oxides, so is not based on their melting or boiling point. Some of the factors influencing joint penetration of TIG welds produced with high thermal stability oxides are not yet completely understood. Moreover, the

* Corresponding author at: No. 1, Hseuhfu Rd., Neipu, Pingtung 91201, Taiwan. Tel.: +886 8 7703202; fax: +886 8 7740552.
E-mail address: tkh@mail.npust.edu.tw (K.-H. Tseng).

http://dx.doi.org/10.1016/j.powtec.2015.07.047
0032-5910/

influences of oxides with high thermal stability on the metallurgical features of HSLA steel TIG weldments have not been widely studied. More research to understand the action of the high thermal stability oxide used in TIG welding of HSLA steel is required. Therefore this study mainly focuses on the high thermal stability oxide assisted TIG welding of AISI 4130 steel.

2. Experimental details

AISI 4130 steel having a nominal composition (in wt.%) of 0.30% C, 0.20% Si, 0.51% Mn, 0.016% P, 0.004% S, 0.83% Cr, 0.17% Mo, and balance Fe was used as the specimen for this study. The dimensional designation of specimen was 100 × 100 × 5 mm. Prior to welding, all specimen surfaces were ground with an abrasive paper to remove impurities, followed by cleaning with acetone.

Five types of powdered oxides (MoO_3, TiO_2, Al_2O_3, MgO, and CaO) were used as the flux for this study. Fig. 1 shows the Ellingham diagram for selected oxides. It can be seen that the Gibbs free energies of formation in Al_2O_3, MgO, and CaO are higher than those in MoO_3 and Cr_2O_3. In other words, Al_2O_3, MgO, and CaO exhibited a relatively strong ability to resist thermal decomposition at high temperature conditions than MoO_3 and Cr_2O_3. Table 1 lists the properties of powdered oxides used for this study. The oxide powders with a particle size of 44–53 μm were separated by dry sieving (retained between 325 and 400 mesh sieves). The powdered oxide was mixed with methanol to attain a flux paste. The paste was applied manually with a paintbrush onto the surface of specimen to be welded. The weight per unit coated area of the flux was 2.52 ± 0.11 mg/cm^2. Methanol was then volatilized within seconds, and a series of bead-on-plate welding trials were subsequently performed.

TIG welding trials were performed using mechanized equipment in which a welding torch with a 3.2 mm diameter, 1.5% lanthanated tungsten electrode (AWS classification EWLa-1.5), was traveled at a constant speed. The included angle of the electrode tip was selected at 60°. The power supply used in TIG welding had a constant-current characteristic. An autogenous, single-pass TIG welding with DCEN polarity was used to make a bead-on-plate weld. The welding current and travel speed were selected to be at 180 A and 150 mm/min, respectively. The arc length was held at 2.0 ± 0.1 mm by using a feeler gauge. High-purity argon was used as the shielding gas and supplied at a flow rate of 12 L/min. During welding, a digital video (DV) recorder was used to monitor the arc voltage values, and a charge-coupled device (CCD) detector was used to capture the image of the arc contour.

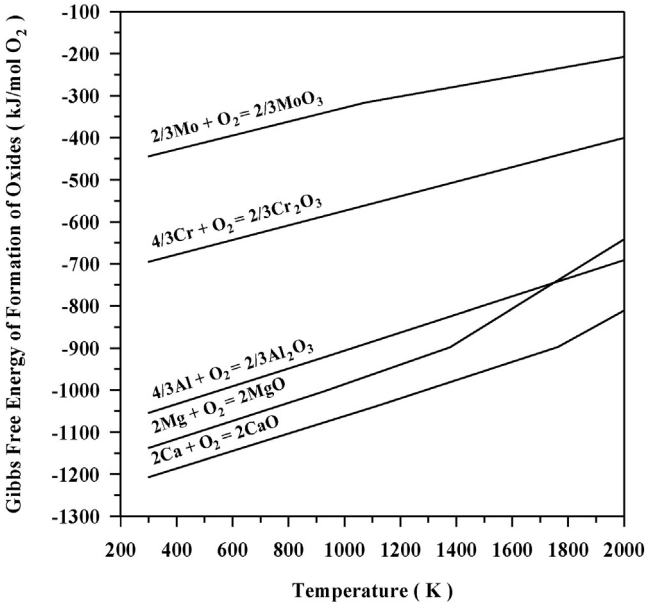

Fig. 1. Ellingham diagram for selected oxides.

Table 1
Properties of powdered oxides used in this study.

Properties	Oxides				
	MoO_3	Cr_2O_3	Al_2O_3	MgO	CaO
Appearance	Gray	Green	White	White	White
Thermal stability	Lower	Lower	Higher	Higher	Higher
Purity (%)	≥99	≥99	≥99	≥99	≥99
Molar mass (g/mol)	143.94	151.99	101.96	40.30	56.08
Mass density (g/cm^3)	4.69	5.22	3.95	3.58	3.30
Melting point (°C)	795	2435	2072	2852	2572
Characteristics	Elements				
	Mo	Cr	Al	Mg	Ca
Electronegativity	1.8	1.6	1.5	1.2	1.0
Work function (eV)	4.60	4.50	4.28	3.66	2.87

After welding, the metallographic samples were sectioned perpendicular to the longitudinal axis of the weld. All samples were prepared using standard operating procedures, including mounting, grinding, rough polishing, fine polishing, followed by etching. Etching was performed using a 2% nital solution. The shape of the weld and the microstructures of the weldment were photographed using an optical microscope. The weld depth (D), bead width (W), and HAZ width of the samples were measured using a Toolmaker's microscope. In this study, the Toolmaker's microscope with monocular head, 30× total magnification, and tungsten illumination created a 2-D image for measuring dimensions of the samples.

Hardness tests were used to evaluate a macroscopic strength of the weldment. The welded specimen was measured in terms of Vickers microhardness under an indentation load of 300 g for 15 s. Microhardness measurements were carried out at regular intervals of 0.25 mm. Also, an oxygen/nitrogen/hydrogen analyzer was used to measure the oxygen concentration in the weld.

3. Results and discussion

3.1. Joint penetration of TIG-PF welding of AISI 4130 steel

Fig. 2 presents the transverse cross-section of AISI 4130 steel TIG welds produced with and without powdered oxides. The cross-sectional size of the fusion zone (FZ) is characterized by the D and W. Fig. 3 shows the geometry size of TIG welds produced with and without powdered oxides. Compared to TIG welding without powdered oxide, using MoO_3 and Cr_2O_3 led to an increase in D and a decrease in W; however, the use of Al_2O_3 and MgO resulted in no significant differences in D and W, but using CaO lead to a decrease in D and an increase in W. Moreover, the cross-sectional shape of the FZ is characterized by the depth/width ratio (DWR) of the weld. Fig. 4 shows the DWR of TIG welds produced with and without powdered oxides. Compared to TIG weld produced without powdered oxide, there was a clear increase in DWR of TIG weld produced with MoO_3 and Cr_2O_3; however, there was no significant difference in DWR of TIG welds produced with Al_2O_3 and MgO, but DWR decreased in TIG weld produced with CaO. A high DWR is the result of a weld having a narrow deep shape; a low DWR is the result of a weld having a wide shallow shape. These results show that using MoO_3 and Cr_2O_3 produced a narrow deep weld, while using Al_2O_3, MgO, and CaO produced a wide shallow weld.

The fluid flow dominates energy transfer within the molten pool, and thus determines the shape and size of the weld. During the arc welding, the liquid metal flow within the molten pool is driven primarily by the gas shear stress (S_S) exerted by the plasma jet (J_P), the Marangoni force (F_M), the Lorentz force (F_L), and the buoyancy force (F_B), as shown in Fig. 5. The actions of the driving forces are based on

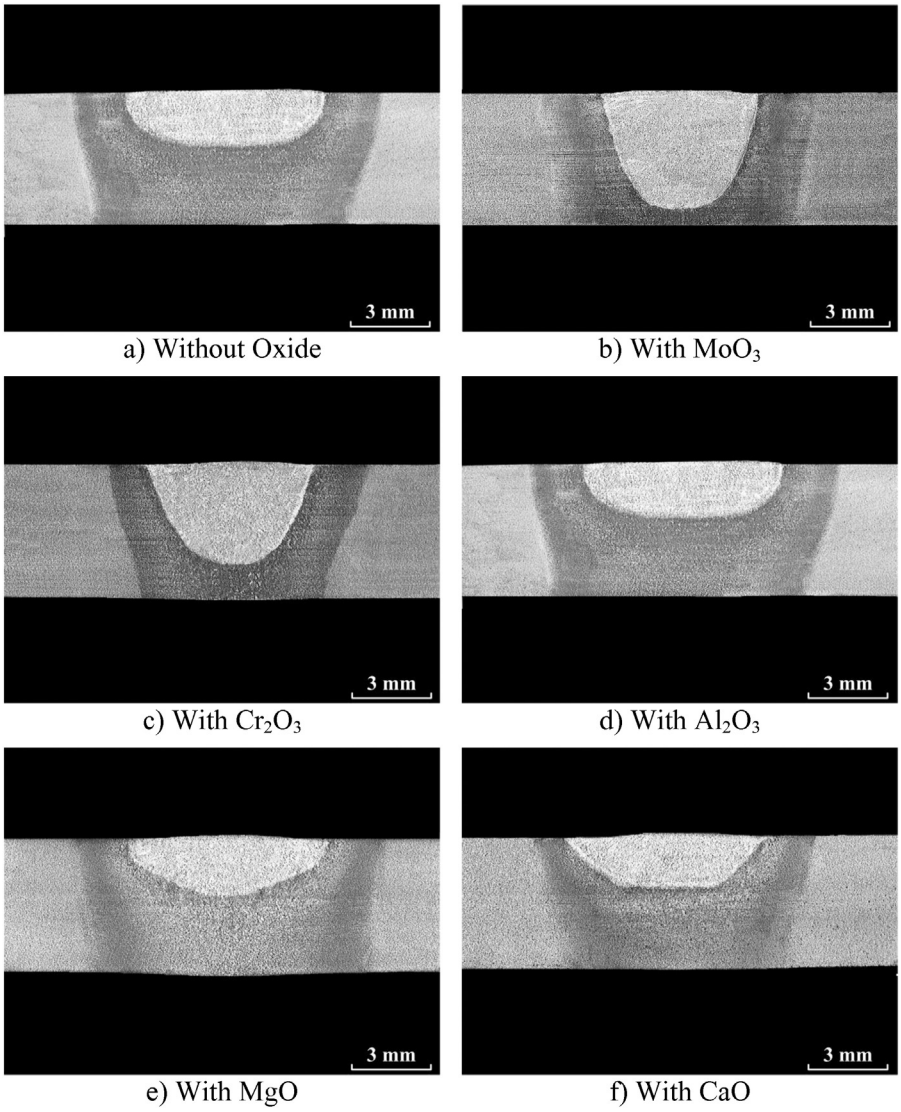

Fig. 2. Transverse cross-section of TIG welds produced with and without powdered oxides.

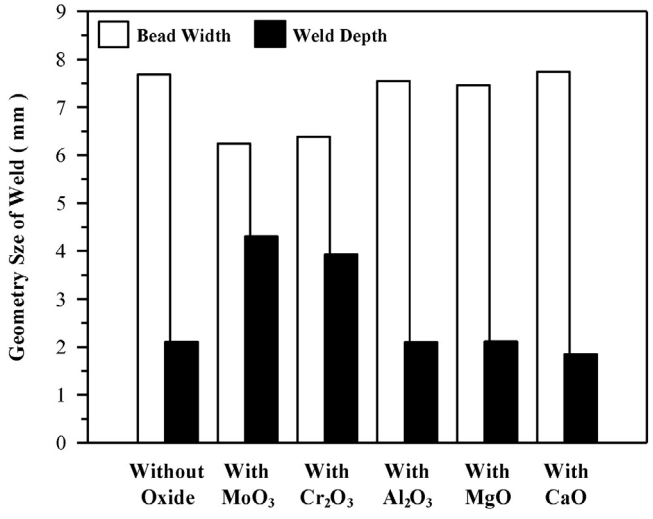

Fig. 3. Geometry size of TIG welds produced with and without powdered oxides.

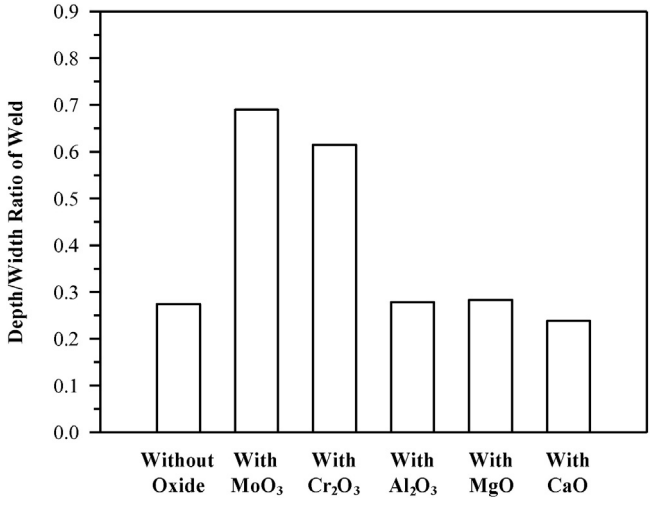

Fig. 4. Depth/width ratio of TIG welds produced with and without powdered oxides.

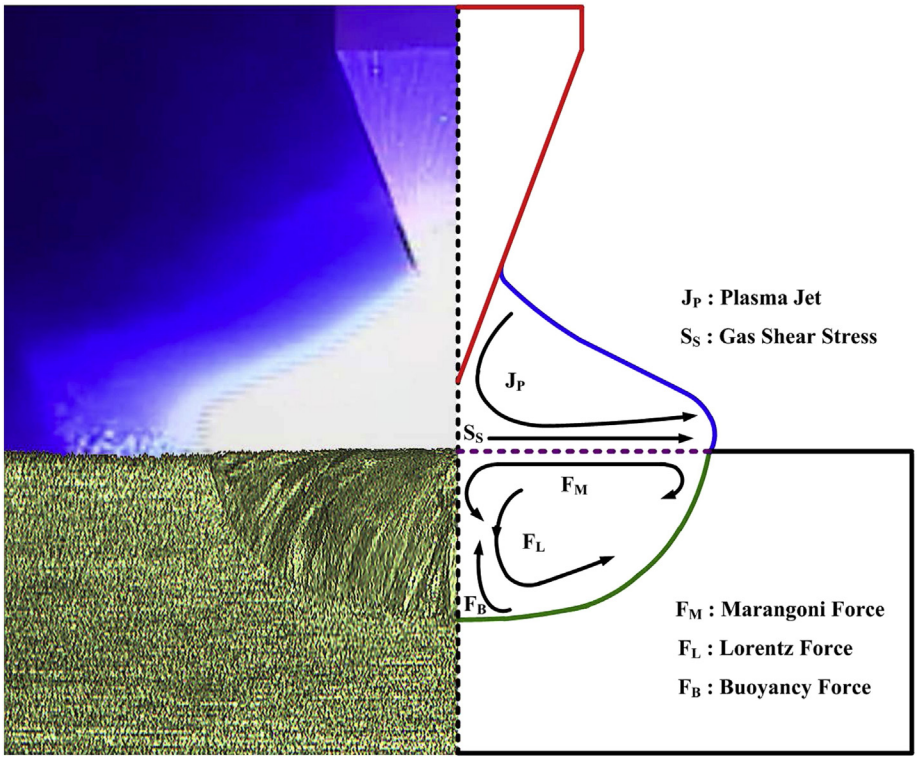

Fig. 5. Driving forces for liquid metal flow in the molten pool.

the net energy balance of the electric arc and molten pool. Note that the difference in distribution of static gas pressure between the electrode and the workpiece produces a J_P toward the workpiece during TIG welding. When the J_P impinges on the molten pool, it will induce the S_S acting on the surface of the molten pool. Thus, the S_S also influences the shape and size of the resulting weld. In addition, the F_B is insignificant during the autogenous TIG welding of steel; it can therefore be ignored, and consideration is instead given to the interaction of the other driving forces in this investigation. Heiple and Roper [16] showed that the presence of oxygen alters the flow of liquid metal by changing the surface tension gradient, and thus reverse the direction of the F_M along the molten pool surface. This reversed F_M promotes the flow of liquid metal from the edge to the central region along the molten pool surface, and the depth of the weld increases dramatically. Moreover, Lucas and Howse [17] showed that the vaporized flux in the peripheral regions of an electric arc exists as the dissociated atoms, which capture the conduction electrons to form charged particles in the peripheral regions of an electric arc. Consequently, the number of conduction electrons in the peripheral regions of an electric arc is reduced. This results in a self-regulated constriction of the electric arc of welding, which has a high current density and leads to an increase in the downward F_L within the molten pool.

Fig. 6 shows the JPA of TIG welds produced with and without powdered oxides. In this study, the JPA of the weld is defined by the percentage variation in the depth of the weld (%ΔD), which can be expressed as

$$\%\Delta D = \frac{D_{w/} - D_{w/o}}{D_{w/o}} \times 100\%$$

where $D_{w/}$ is the depth of the weld produced with powdered oxide and $D_{w/o}$ is the depth of the weld produced without powdered oxide.

Using MoO_3 and Cr_2O_3 significantly improves the JPA of AISI 4130 steel TIG welds compared to using Al_2O_3, MgO, and CaO. Experimental results of dissolved oxygen concentration (DOC) and arc divergence angle (ADA) have been discussed here to explain the influence of high and low thermal stability oxides on the JPA of AISI 4130 steel welds.

The presence of the dissolved oxygen in molten metal, generated by the thermal decomposition of the powdered oxide, influences the F_M within the molten pool. Fig. 7 shows the DOC in TIG welds produced with and without powdered oxides. The results presented in this study show that the DOC in AISI 4130 steel TIG weld produced without powdered oxide was 20 ppm. The DOC in the welds produced with MoO_3 and Cr_2O_3 range from 40 ppm to 55 ppm. This study presumed that sufficient dissolved oxygen exists in the molten metal produced with MoO_3 and Cr_2O_3, and thus the F_M along the molten pool surface changes from outward to inward flow. Nevertheless, the DOC in the welds produced with Al_2O_3, MgO, and CaO range from 14 ppm to 19 ppm, resulting in insufficient dissolved oxygen in the molten metal. As seen in Fig. 1, Al_2O_3, MgO, and CaO are more thermodynamically stable. These oxides cannot be completely decomposed by the arc heat of TIG welding to create sufficient dissolved oxygen in AISI 4130 steel

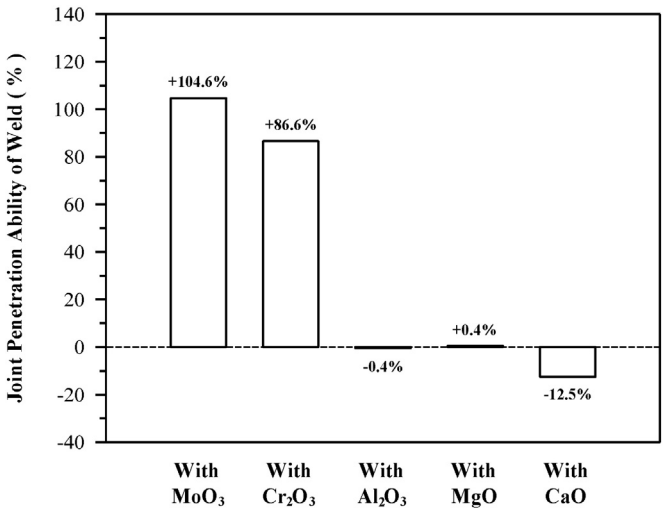

Fig. 6. Joint penetration ability of TIG welds produced with and without powdered oxides.

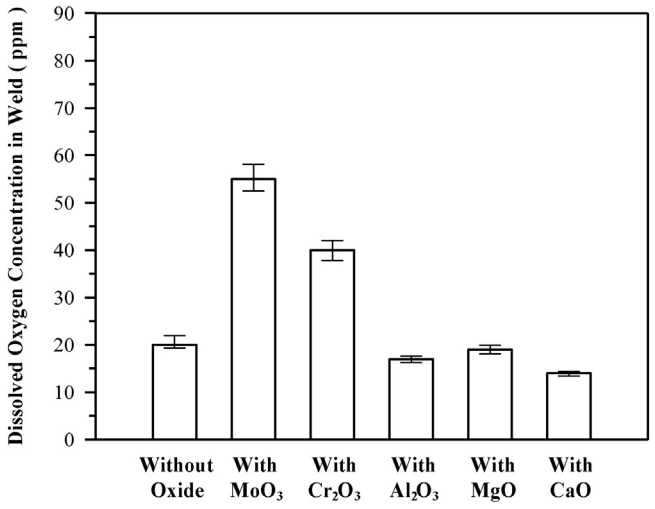

Fig. 7. Dissolved oxygen concentration in TIG welds produced with and without powdered oxides.

molten metal. In addition, Al, Mg, and Ca were commonly used as deoxidizers in the steelmaking, and thus the DOC in the welds produced with Al_2O_3, MgO, and CaO was lower than that in the welds produced without powdered oxide. Consequently, the direction of the F_M is not reversed to go inward along the molten pool surface. It should be noted that MgO exhibits a higher thermal stability than Al_2O_3 at temperatures below 1740 K, while MgO exhibits a lower thermal stability than Al_2O_3 at temperatures above 1740 K. Kraus [20] reported that the peak temperatures at the molten pool surface range from 2200 K to 3000 K for the stationary TIG welding of steels. MgO is easily decomposed by TIG welding arc under heating temperatures of above 1740 K, resulting in a slightly higher DOC in AISI 4130 steel TIG weld produced with MgO (19 ppm) compared to TIG weld produced with Al_2O_3 (17 ppm).

The change in the arc contour of TIG welding, produced by thermal dissociation of powdered oxide, influences the F_L within the molten pool. Fig. 8 shows the ADA for TIG welding with and without powdered oxides. The arrangement of ADA for TIG welding is shown in Fig. 9. Compared to TIG welding without powdered oxide, there was a decrease in ADA resulting from the use of MoO_3 and Cr_2O_3; however, the use of Al_2O_3 and MgO results in no significant differences in ADA, but the use of CaO leads to an increase in ADA. A small ADA is responsible for the constricted contour of an electric arc of TIG welding; a large ADA is responsible for the expanded contour of an electric arc of TIG welding.

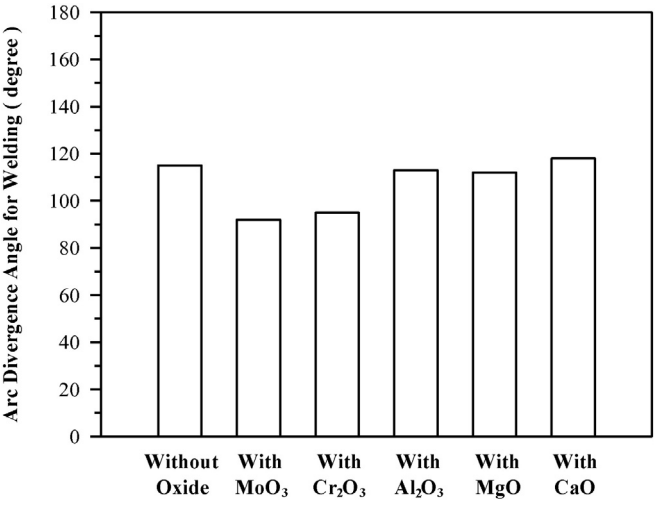

Fig. 8. Arc divergence angle for TIG welding with and without powdered oxides.

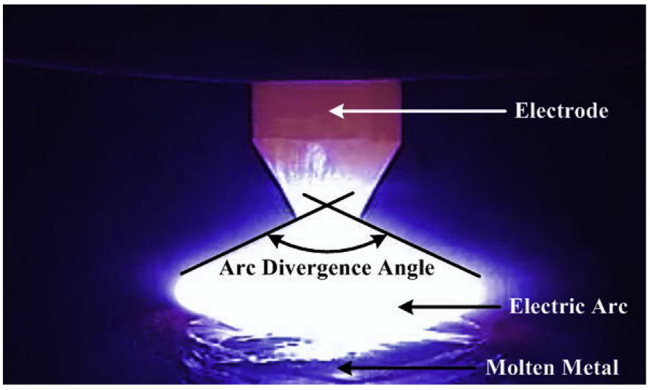

Fig. 9. Arrangement of arc divergence angle for TIG welding.

The results show that the use of MoO_3 and Cr_2O_3 produced a constricted arc contour, while the use of Al_2O_3, MgO, and CaO produced an expanded arc contour. Tseng and Hsu [12] reported that the variation in arc voltage of TIG welding reflected the contour of an electric arc. It was observed that arc voltage increased when the arc contour of low thermal stability oxide assisted TIG welding was constricted. Fig. 10 shows the arc voltage for TIG welding with and without powdered oxides. Compared to TIG welding without powdered oxide, there was an increase in arc voltage resulting from the use of MoO_3 and Cr_2O_3; however, the use of Al_2O_3 and MgO results in no significant differences in arc voltage, but the use of CaO leads to a decrease in arc voltage. The result of the measured arc voltage is direct proof that the arc contour for TIG welding with Al_2O_3, MgO, and CaO is broader than that for TIG welding with MoO_3 and Cr_2O_3 at the same arc current and arc length. The constricted arc contour of TIG welding increases the downward F_L within the molten pool.

It was concluded that the MoO_3 and Cr_2O_3 could increase downward F_L together with a reversed F_B within the molten pool. This resulted in an effective transfer of thermal energy from the edge of the molten pool surface to its center, and then downwards to the bottom of the molten pool [18]. Consequently, we expected a greater improvement in the JPA of the weld in the MoO_3 and Cr_2O_3 assisted TIG welding of AISI 4130 steel. In contrast, Al_2O_3, MgO, and CaO did not benefit the increase in the downward F_L within the molten pool and reversing the direction of FB along the molten pool surface. Thus, TIG welding with Al_2O_3, MgO, and CaO did not considerably improve the JPA of AISI 4130 steel welds compared to TIG welding without powdered oxide.

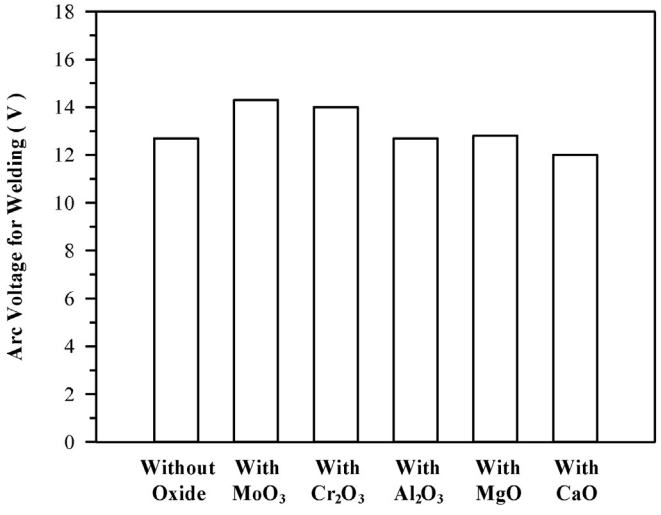

Fig. 10. Arc voltage for TIG welding with and without powdered oxides.

As seen in Fig. 6, CaO had a greater negative effect on the JPA of AISI 4130 steel TIG weld, as compared to TIG welds produced by Al_2O_3 and MgO. The work function of Ca (2.87 eV) was lower than that of Al (4.28 eV) and Mg (3.66 eV) [19]. Thus, the number of conduction electrons in the peripheral regions of an electric arc of TIG welding with CaO may increase. In other words, the arc contour for TIG welding with CaO is broader than that for TIG welding with Al_2O_3 and MgO, further reducing the downward F_L within the molten pool and increasing the outward S_S acting on the top surface of the molten pool. This decreases the D and increases the W compared to TIG welding with Al_2O_3 and MgO under the same welding conditions (Fig. 3).

Based on the results of the present study, the thermal stability of the powdered oxide is a key factor in determining the JPA of TIG-PF weld. The use of MoO_3 and Cr_2O_3 could significantly improve the JPA of AISI 4130 steel TIG weld, while the use of Al_2O_3 and MgO did not increase the JPA of the welds. In particular, the use of CaO, which has a greater thermodynamically stability and lower work function, caused a decrease in JPA of the weld. Moreover, the use of Al_2O_3, MgO, or CaO may lead to the formation of a compact, continuous slag floating on the surface of molten metal, acting as a barrier for thermal energy transfer from the electric arc to the molten pool during TIG-PF welding. Fig. 11 shows the mechanism for determining the JPA of TIG welds produced with powdered oxides under various thermal stabilities.

Stout et al. [21] reported that high oxygen concentration in the weld has a negative effect on the notch toughness of high strength steel weldment. Note that TIG welding with low thermal stability oxide readily caused too-high DOC in the weld. To improve both joint penetration and notch toughness of high strength steel weldment, small additions of Al_2O_3, MgO, or CaO may be useful in controlling the DOC in HSLA steel TIG-PF welds.

3.2. Metallurgical feature of TIG-PF welding of AISI 4130 steel

Experimental results of microstructure and microhardness are discussed here to explain the influences of high and low thermal stability oxides on the metallurgical feature of AISI 4130 steel TIG weldments. Fig. 12 shows that the base metal (BM) is mainly composed of ferrite (bright) and pearlite (dark), which shows a typical microstructure of hot-rolled HSLA steel and a microhardness value range from 190 H_V to 210 H_V. Fig. 13 presents the microstructure and microhardness of AISI 4130 steel TIG weldments. The metallurgical features of the HAZ are

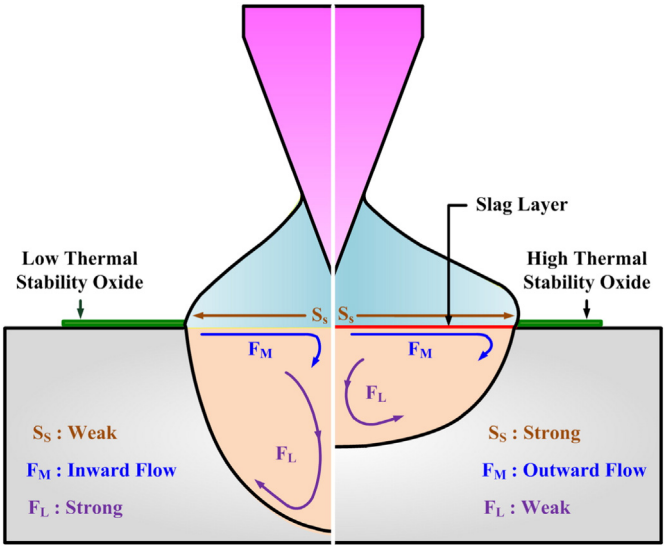

Fig. 11. Mechanism for determining JPA of TIG welds produced with powdered oxides under various thermal stabilities.

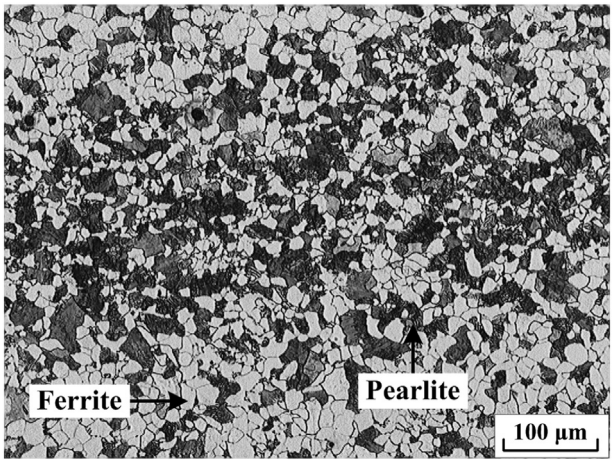

Fig. 12. Typical microstructure of AISI 4130 steel base metal.

different from those of the BM due to the welding thermal cycle. During welding, the HAZ was subjected to different cooling rates, and thus it exhibited heterogeneous phase structures and distributions of hardness. In this study, the HAZ in AISI 4130 steel TIG weldment can be divided into three distinct subregions with obviously various microstructures: intercritical HAZ (ICHAZ), fine-grained HAZ (FGHAZ), and coarse-grained HAZ (CGHAZ). The ICHAZ has the lowest microhardness value (230–300 H_V) in the HAZ of TIG weldment produced without powdered oxide. The microstructure of the ICHAZ consists of ferrite and pearlite. Note that the BM has fine ferrite, while the ICHAZ has fine pearlite. The FGHAZ of TIG weldment produced without powdered oxide has an average microhardness value of 340 H_V. The microstructure of the FGHAZ consists of ferrite and martensite/austenite constituent. The CGHAZ has the highest microhardness value (370–390 H_V) in the HAZ of TIG weldment produced without powdered oxide. The microstructure of the CGHAZ consists of ferrite and martensite. Note that the CGHAZ contains a higher proportion of martensite, while the FGHAZ contains a higher proportion of ferrite. The results indicat that the CGHAZ of AISI 4130 steel TIG weldment can form martensite, the HAZ of which has a high microhardness. In other words, AISI 4130 steel has a relatively high hardenability. Lastly, the microstructure of the WM is mainly composed of martensite, and its microhardness value (420–435 H_V) is highest in TIG weldment produced without powdered oxide. In this study, the highest hardness is located in the WM, which is followed by the CGHAZ, FGHAZ, and ICHAZ, while the lowest hardness is located in the BM. Furthermore, the hard microstructures formed in the WM and CGHAZ of AISI 4130 steel weldment exhibited a considerable microhardness value (>370 Hv).

As observed in Fig. 13, the WM and HAZ in TIG weldment produced with MgO or MoO_3 have approximately the same microstructure and microhardness, as compared to TIG weldment produced without powdered oxide. The results show there are no significant differences in the metallurgical features of TIG weldment produced with high or low thermal stability oxide, as compared to TIG weldment produced without powdered oxide. Fig. 14 shows the HAZ width of TIG weldments produced with and without powdered oxides. Compared to TIG welding without powdered oxide, there was a decrease in HAZ width resulting from the use of MoO_3 and Cr_2O_3. However, the use of Al_2O_3, MgO, and CaO results in no significant differences in HAZ width. TIG welding with MoO_3 and Cr_2O_3 increased the D and DWR, which indicates that the TIG welding arc has a higher energy density. This resulted in a decrease in heat loss of TIG welding arc and an increase in melting efficiency. This contributed to reducing the amount of thermal energy dissipated to the HAZ. Consequently, the HAZ width of TIG weldments produced with MoO_3 and Cr_2O_3 became relatively narrow compared to TIG weldments produced with Al_2O_3, MgO, and CaO.

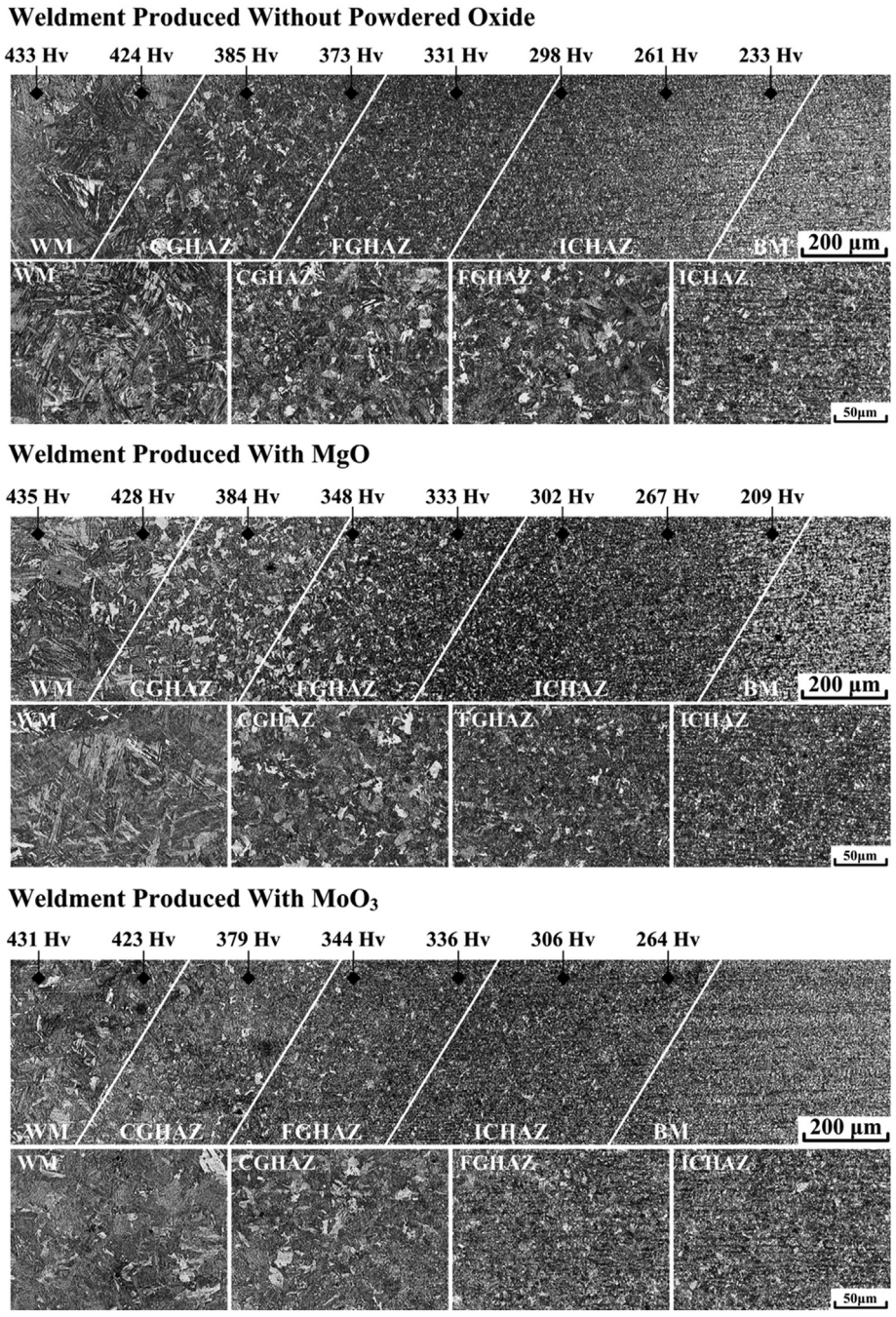

Fig. 13. Microstructure and microhardness of AISI 4130 steel weldments.

4. Conclusions

The influences of MoO_3, Cr_2O_3, Al_2O_3, MgO, and CaO powders on the joint penetration and metallurgical feature of AISI 4130 steel TIG-PF weldments were investigated. This study also offers an explanation for the integrated mechanism that determines the JPA of TIG welds produced with various thermal stability oxides. The findings presented in this study are summarized below:

1. TIG welding with MoO_3 or Cr_2O_3 increases downward Lorentz flow together with a reversed Marangoni convection within the molten pool. This greatly improves the joint penetration of AISI 4130 steel weld, as compared to TIG weld produced without powdered oxide.
2. TIG welding with Al_2O_3 and MgO did not contribute significantly to increasing the Lorentz flow or reversing the Marangoni convection. Consequently, there was no significant difference in the joint penetration of AISI 4130 steel weld compared to TIG weld produced without powdered oxide.
3. The work function of Ca is lower than that of Al and Mg. The use of CaO broadened the arc contour of TIG welding, further reducing the downward Lorentz flow and increasing the outward gas shear flow in the molten pool. As a result, the shape of the resulting weld became relatively shallow and wide compared to TIG weld produced without powdered oxide.
4. TIG welding with high thermal stability oxides may generate a heavy slag floating on the surface of molten metal. The heavy slag layer hinders thermal energy transfer from the electric arc to the molten pool during TIG-PF welding.
5. Looking at the microstructure and microhardness of AISI 4130 steel TIG weldment produced with or without powdered oxide, the

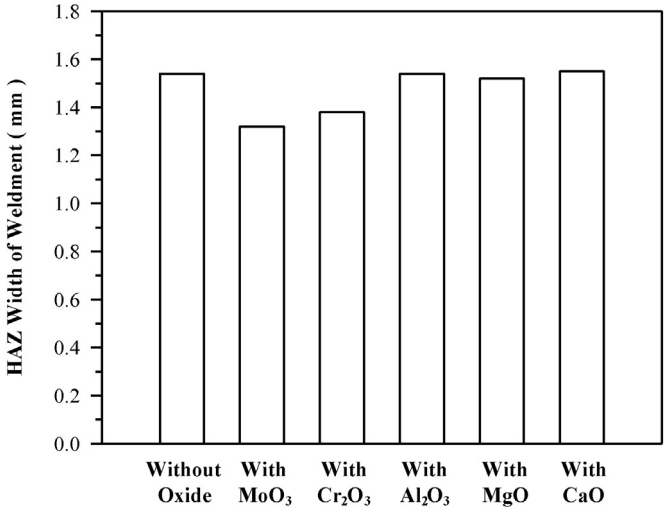

Fig. 14. HAZ width of TIG weldments produced with and without powdered oxides.

microstructure of the BM consists of ferrite and pearlite, which has the lowest microhardness. The microstructure of the HAZ consists of ferrite, pearlite, and martensite/austenite, which reveals a heterogeneous distribution of microhardness in the weldment. The microstructure of the WM mainly consists of martensite, which has the highest microhardness.

6. The hard microstructures formed in the WM and CGHAZ of AISI 4130 steel weldment exhibited a considerable microhardness value (>370 H_V).

Acknowledgments

The authors gratefully acknowledge the financial support provided to this study by the Ministry of Science and Technology, Taiwan under grant no. 103-2622-E-020-007-CC3.

References

[1] A. Emamian, A. Emamian, A.H. Kowkabi, Effects of fillerwire composition along with different pre- and post-heat treatment on mechanical properties of AISI 4130 welded by the GTAW process, Mater. Sci. Appl. 1 (2010) 135–140.
[2] H. Bultel, J.B. Vogt, Influence of heat treatment on fatigue behaviour of 4130 AISI steel, Procedia Eng. 2 (2010) 917–924.
[3] K.H. Tseng, K.L. Chen, Comparisons between TiO_2- and SiO_2-flux assisted TIG welding processes, J. Nanosci. Nanotechnol. 12 (2012) 6359–6367.
[4] K.H. Tseng, N.S. Wang, GTA welding assisted by mixed ionic compounds of stainless steel, Powder Technol. 251 (2014) 52–60.
[5] H.L. Lin, T.M. Wu, C.M. Cheng, Effects of flux precoating and process parameter on welding performance of Inconel 718 alloy TIG welds, J. Mater. Eng. Perform. 23 (2014) 125–132.
[6] T. Sándor, C. Mekler, J. Dobránszky, G. Kaptay, An improved theoretical model for A-TIG welding based on surface phase transition and reversed Marangoni flow, Metall. Mater. Trans. A 44 (2013) 351–361.
[7] T.S. Chern, K.H. Tseng, H.L. Tsai, Study of the characteristics of duplex stainless steel activated tungsten inert gas welds, Mater. Des. 32 (2011) 255–263.
[8] P.J. Modenesi, E.R. Apolinário, I.M. Pereira, TIG welding with single-component fluxes, J. Mater. Process. Technol. 99 (2000) 260–265.
[9] K.H. Tseng, Development and application of oxide-based flux powder for tungsten inert gas welding of austenitic stainless steels, Powder Technol. 233 (2013) 72–79.
[10] S.P. Lu, H. Fujii, H. Sugiyama, K. Nogi, Mechanism and optimization of oxide fluxes for deep penetration in gas tungsten arc welding, Metall. Mater. Trans. A 34 (2003) 1901–1907.
[11] H.Y. Huang, S.W. Shyu, K.H. Tseng, C.P. Chou, Effects of the process parameters on austenitic stainless steel by TIG-flux welding, J. Mater. Sci. Technol. 22 (2006) 367–374.
[12] K.H. Tseng, C.Y. Hsu, Performance of activated TIG process in austenitic stainless steel welds, J. Mater. Process. Technol. 211 (2011) 503–512.
[13] K.H. Tseng, K.J. Chuang, Application of iron-based powders in tungsten inert gas welding for 17Cr–10Ni–2Mo alloys, Powder Technol. 228 (2012) 36–46.
[14] K.H. Tseng, P.Y. Lin, UNS S31603 stainless steel tungsten inert gas welds made with microparticle and nanoparticle oxides, Materials 7 (2014) 4755–4772.
[15] S. Tathgir, A. Bhattacharya, T.K. Bera, Influence of current and shielding gas in TiO_2 flux activated TIG welding on different graded steels, Mater. Manuf. Process. 30 (2015) 1115–1123.
[16] C.R. Heiple, J.R. Roper, Mechanism for minor element effect on GTA fusion zone geometry, Weld. J. 61 (1982) 97–102.
[17] W. Lucas, D. Howse, Activating flux-increasing the performance and productivity of the TIG and plasma processes, Weld. Met. Fabr. 64 (1996) 11–17.
[18] K.H. Tseng, P.Y. Chen, Effect of TiO_2 crystalline phase on performance of flux assisted GTA welds, Mater. Manuf. Process. (2015), http://dx.doi.org/10.1080/10426914.2015.1058952.
[19] H.B. Michaelson, The work function of the elements and its periodicity, J. Appl. Phys. 48 (1977) 4729–4733.
[20] H.G. Kraus, Experimental measurement of stationary SS 304, SS 316 and 8630 GTA weld pool surface temperatures, Weld. J. 68 (1989) 269–279.
[21] R.D. Stout, P.M. Machmeir, R. Quattrone, Effects of impurities on properties of high-strength steel weld metal, Weld. J. 49 (1970) 521–530.